JOURNAL OF VIROLOGY, Aug. 1997, p. 6155–6167 Vol. 71, No. 8
0022-538X/97/$04.00+0

Sequence and Structure Alignment of *Paramyxoviridae* Attachment Proteins and Discovery of Enzymatic Activity for a Morbillivirus Hemagglutinin

JOHANNES P. M. LANGEDIJK,* FRANZ J. DAUS, AND JAN T. VAN OIRSCHOT

Department of Mammalian Virology, The Institute for Animal Science and Health (ID-DLO), Lelystad, The Netherlands

Received 21 January 1997/Accepted 9 May 1997

On the basis of the conservation of neuraminidase (N) active-site residues in influenza virus N and paramyxovirus hemagglutinin-neuraminidase (HN), it has been suggested that the three-dimensional (3D) structures of the globular heads of the two proteins are broadly similar. In this study, details of this structural similarity are worked out. Detailed multiple sequence alignment of paramyxovirus HN proteins and influenza virus N proteins was based on the schematic representation of the previously proposed structural similarity. This multiple sequence alignment of paramyxovirus HN proteins was used as an intermediate to align the morbillivirus hemagglutinin (H) proteins with neuraminidase. Hypothetical 3D structures were built for paramyxovirus HN and morbillivirus H, based on homology modelling. The locations of insertions and deletions, glycosylation sites, active-site residues, and disulfide bridges agree with the proposed 3D structure of HN and H of the *Paramyxoviridae*. Moreover, details of the modelled H protein predict previously undescribed enzymatic activity. This prediction was confirmed for rinderpest virus and peste des petits ruminants virus. The enzymatic activity was highly substrate specific, because sialic acid was released only from crude mucins isolated from bovine submaxillary glands. The enzymatic activity may indicate a general infection mechanism for respiratory viruses, and the active site may prove to be a new target for antiviral compounds.

The family *Paramyxoviridae* contains three genera: *Paramyxovirus* (Sendai virus, parainfluenza virus type I [PIV-1], and PIV-3, mumps virus, simian virus type 5 [SV-5], Newcastle disease virus [NDV], PIV-2, and PIV-4), *Morbillivirus* (measles virus, rinderpest virus [RPV], and the distemper viruses phocine distemper virus phocine distemper virus [PDV] and canine distemper virus [CDV]), and *Pneumovirus*. The *Pneumovirinae* are classified as a separate genus because of differences in the diameter of the nucleocapsid and the lack of detectable hemagglutination and neuraminidase (N) activity (27, 49). They also differ in aspects of viral RNA and protein structure (7).

The *Paramyxoviridae* are enveloped viruses that contain two envelope glycoproteins, the fusion protein (F) and the attachment protein (hemagglutinin-neuraminidase [HN], hemagglutinin [H], or G). The attachment protein HN of paramyxoviruses contains both hemagglutination and neuraminidase (sialidase) activity, like influenza virus N, and binds and cleaves terminal sialic acids. The attachment protein (H) of morbilliviruses has hemagglutinin activity, but neuraminidase activity has never been described.

H and HN are globular proteins of the same size, and the positions of these attachment proteins in the genome organization are conserved. The function of the neuraminidase activity of viruses is not well understood. It has been shown that influenza virus N is necessary to facilitate the release of progeny virus from infected cells (47). Cleavage of sialic acids releases the virus from the glycosylated cellular membrane proteins. Another possible role of the neuraminidase may be the transport of the virus through the sialic acid-rich mucus layer that protects internal body parts from harmful agents. This role will be discussed in this paper.

It has been demonstrated for several paramyxoviruses that HN is necessary for the initial fusion. It has been proposed that F and HN act in concert to establish infection; however, the requirement for HN for this process is still questioned (reviewed in reference 28). Furthermore, a type-specific functional interaction between F and HN of some paramyxoviruses is required (3, 13, 22, 52). Similarly, a specific interaction is proposed for F and H of a morbillivirus (5).

In this study, we compared the sequence and structure of morbillivirus H with parainfluenza virus HN, influenza virus N, bacterial neuraminidases, eukaryotic neuraminidase, and protozoan transneuraminidases. The crystal structures of the neuraminidases of influenza viruses A and B, *Salmonella typhimurium* LT2, and *Vibrio cholerae* show the same fold and a remarkable similarity in the spatial arrangement of the catalytic residues, although the sequence similarity is low (4, 11, 12, 56). Seven active-site residues are common in most of these neuraminidases: R118, D151, E277, R292, R371, Y406, and E425, according to the numbering of influenza virus A/Tokyo/3/67 (58). All resolved neuraminidase structures are organized as a so-called β-propeller. This is a superbarrel comprising six similarly folded antiparallel β-sheets of four strands each. In the superbarrel, the six sheets are arranged cyclically around an axis through the center of the molecule like the blades of a propeller. The center of the molecule forms the active site and binds sialic acid. Also, the way the sheets are connected is conserved: the fourth strand of each sheet is connected across the top of the molecule to the first strand of the next sheet. A notation for the secondary structure elements of the subunit is $\beta_i S_j$ or $\beta_i L_{mn}$ where $i = 1$ to 6 for the six β-sheets and $j = 1$ to 4 for the four strands per sheet and where the loop structures are designated L01, L12, L23, and L34, which refer to, respectively, the loop connecting strand 4 of the preceding sheet with

* Corresponding author. Present address: Department of Molecular Biology, The Scripps Research Institute, 10550 N. Torrey Pines Rd., La Jolla, CA 92037. Phone: (619) 784-8159. Fax: (619) 784-2980. E-mail: hansl@scripps.edu.

strand 1 of the next sheet (L01) and the loops connecting strand 1 with strand 2 (L12), strand 2 with strand 3 (L23), and strand 3 with strand 4 (L34). Loops L01 and L23 protrude from the top surface, and loops L12 and L34 are on the bottom surface. Because sialic acid binds to the top center of the molecule, active-site residues are located on S_1, L01, and L23.

On the basis of multiple sequence alignment of a diverse set of neuraminidases, three-dimensional (3D) models were built for *paramyxoviridae* HN and H. The validity of the models was checked with published experimental data. The 3D model of morbillivirus H predicted glycosidic activity which was proven for RPV and peste des petits ruminants virus (PPRV).

MATERIALS AND METHODS

Cells and viruses. RPV strain RBOK, PPRV (kindly provided by J. Anderson, Pirbright, United Kingdom), measles virus strain Edmonston (16), PDV strain 1-3 (fourth passage), CDV strain Rockborn (first passage), dolphin morbillivirus (DMV) strain 16A (seventh passage), and bovine respiratory syncytial virus (BRSV) strain RB94 were grown on Vero cells. (Measles virus, PDV, CDV, and DMV were kindly provided by A. D. M. E. Osterhaus, Erasmus University, Rotterdam, The Netherlands.) Infected cell cultures were maintained in Eagle's minimum essential medium with 2% fetal bovine serum. Virions were obtained by clarification of tissue culture medium. The virions were further purified by pelleting the clarified medium through a 40% sucrose cushion at 250,000 × *g* for 20 min. In some experiments, the clarified medium was pelleted without sucrose at 53,000 × *g* for 2 h, giving the same results.

Sequence analysis. Multiple sequence alignments were performed by using the Pileup program of the Genetics Computer Group (14) which was obtained from the CAOS CAMM Centre in Nijmegen, The Netherlands. Several scoring matrices were used: the Dayhoff matrix based on mutations in protein families and a structural matrix based on possible dihedral angles a residue can adopt in folded proteins (45). Multiple sequence alignments were performed with several representative sequences of neuraminidase family members and morbillivirus H proteins, because the use of a broad family of homologous sequences improves the accuracy of structure predictions. Secondary-structure predictions were performed with the neural-network-based program PHD (51), which was obtained from the European Molecular Biology Laboratories in Heidelberg, Germany. The following neuraminidase, HN, or H sequences were obtained from the CAOS CAMM Centre for analysis and comparison: *V. cholerae* Ogawa neuraminidase (accession no. P37060), *Actinomyces viscosus* DSM 43798 neuraminidase (S20590), *Trypanosoma cruzi* flagellum-associated protein (S32016), *S. typhimurium* LT2 neuraminidase (P29768), *Clostridium septicum* NC 0054714 neuraminidase (P29767), rat cytosolic neuraminidase (42), influenza A virus strain A/NT/60/68 neuraminidase (A00885), influenza B virus strain B/Beijing/1/87 neuraminidase (B38520), human PIV-2 strain Toshiba hemagglutinin-neuraminidase (A33777), NDV strain Beaudette C/45 hemagglutinin-neuraminidase (A27005), Sendai virus strain HVJ hemagglutinin-neuraminidase (A24004), bovine PIV-3 (bPIV-3) hemagglutinin-neuraminidase (B27218), CDV strain Onderstepoort hemagglutinin (A38480), and measles virus strain Edmonston hemagglutinin (A27006).

Molecular modelling was performed by using software of SYBYL, version 6.0 (Tripos Associates, St. Louis, Mo.) on a Silicon Graphics Indigo computer. Energy minimization was performed with the Tripos SYBYL version 6.0 force field. Minimization was performed by using a dielectric constant, ε, of 1. Minimization was performed in stages using steepest descent and conjugate gradient; at each stage, the atoms were given more freedom as described elsewhere (34). For the introduction of insertions and deletions in the model structure, the program LOOP SEARCH in the SYBYL package was used. The loop regions were taken from a protein fragment database, and the selection was based on the correct length, maximum amino acid homology, and minimum root mean square difference of the anchor residues in the start and the end of the loop.

Neuraminidase assays. Neuraminidase assays were performed as described by Aymard-Henry et al. (1), using different morbilliviruses grown on Vero cells. A 50-μl volume of purified virus was added to 50 μl of the substrates and 100 μl of buffer, and the mixture was incubated for 18 h at 37°C. The following substrates were tested for sialic acid release: fetuin from fetal calf serum (M-2379; Sigma, St. Louis, Mo.) at 50 mg/ml; mucin type 1, isolated from bovine submaxillary glands (M-4503; Sigma), at 50 mg/ml (in some experiments, 100 mg/ml was used, and then the solute was clarified); mucin type 1-S, isolated from bovine submaxillary glands and further purified (M-3895; Sigma), at 50 mg/ml; mucin type 2, isolated from porcine stomach (M-2378; Sigma), at 50 mg/ml; 6′-*N*-acetylneuraminlactose from bovine colostrum (A-8681; Sigma) at 10 mg/ml; 3′-*N*-acetylneuraminlactose from bovine colostrum (A-8556; Sigma) at 10 mg/ml; bovine hyaluronic acid (H-7630; Sigma) at 50 mg/ml; and human hyaluronic acid (H-1751; Sigma) at 50 mg/ml. Neuraminidase from *Clostridium perfringens* (N-2876; Sigma) was used as a positive control.

Hemadsorption test. Hemadsorption tests were performed at 20°C as described previously (57). Vero cells were infected with measles virus strain Edmonston. Erythrocytes of *Cercopithecus* monkeys were a kind gift of P. de Vries of the National Institute of Public Health and the Environment, Bilthoven, The Netherlands.

RESULTS

Multiple sequence alignments were performed with several representative neuraminidase sequences of influenza viruses A and B and several representative HN sequences of paramyxoviruses (Fig. 1) in order to combine the two separate multiple sequence alignments of influenza virus N and paramyxovirus HN described by Colman et al. (9). Alignments were performed by using diverse parameters for gap-weight and gap-length-weight and two different similarity matrices (Materials and Methods). Parts of the computer-generated alignments were combined manually in a final alignment in such a way that the active-site residues as described by Colman et al. (9) were properly aligned. Manual editing of the alignment was also assisted by a neural-network-based secondary-structure prediction (51) which was occasionally used as a guideline to align sequence blocks with low homology. If possible, gaps were avoided in regions corresponding to strands in the influenza virus N molecule. The presented alignment (Fig. 1) between influenza virus N and parainfluenza virus HN could not be generated by using only the computer, because none of the cysteine residues match between influenza viruses and parainfluenza viruses. Because these residues have a very high score in the similarity matrix, the computer-generated alignment was incorrectly biased.

The alignment was extended with the multiple sequence alignment of bacterial, protozoan, and eukaryotic neuraminidases. The correct alignment of the bacterial and protozoan neuraminidases with the viral neuraminidases was based on the structural alignment of influenza virus N and *S. typhimurium* N as described by Crennell et al. (12), which was based on topologically equivalent residues. Finally, the multiple sequence alignment of paramyxovirus HN was used as an intermediate set of sequences to align the morbillivirus H proteins with all other neuraminidases (Fig. 1). β6S4 of morbillivirus H and paramyxovirus HN are homologous according to a circular alignment (Fig. 1).

Although the similarity of the primary sequence of bacterial neuraminidases to the primary sequence of influenza virus neuraminidase was very low (7.3 to 11%) (Table 1), the crystal structures of *V. cholerae* neuraminidase and *S. typhimurium* neuraminidase show the same fold as influenza virus neur-

FIG. 1. Alignment of bacterial, protozoan, eukaryotic, and viral neuraminidases. The strands of β-sheets 1 to 6 are colored from purple (N terminus) to cyan (C terminus). Strands are colored purple in sheet 1, magenta in sheet 2, red in sheet 3, orange in sheet 4, green in sheet 5, and cyan in sheet 6. β-Strands are assigned according to 3D structures of *S. typhimurium* neuraminidase and influenza virus A neuraminidase. Cystine bridges in influenza viruses A and B (green lines), proposed cystine bridges in the *Paramyxovirinae* (blue lines), and connections of long-range disulfide bonds (circles and boxes, respectively) are indicated. Proposed disulfide bonds in *Paramyxovirinae* are based on structural models in Fig. 3a and b. Active-site residues (in red, numbered 1 to 7), conserved residues in respective columns (capital letters), and unaligned protein domains (square boxes) are also shown. Large inserts (diamond-shaped boxes) with their lengths given in parentheses and gaps (periods) are indicated. Residue numbering is indicated after each line. Crystal structures are known for neuraminidases of *V. cholerae*, *S. typhimurium*, and influenza viruses A and B. TM, transmembrane region; tryp-cruz., *T. cruzi*; sal-typh., *S. typhimurium*; clos-sept., *C. septicum*; infl-a and infl-b, influenza A and B virus, respectively; pi-ii, PIV-2; bpi-iii, bPIV-3.

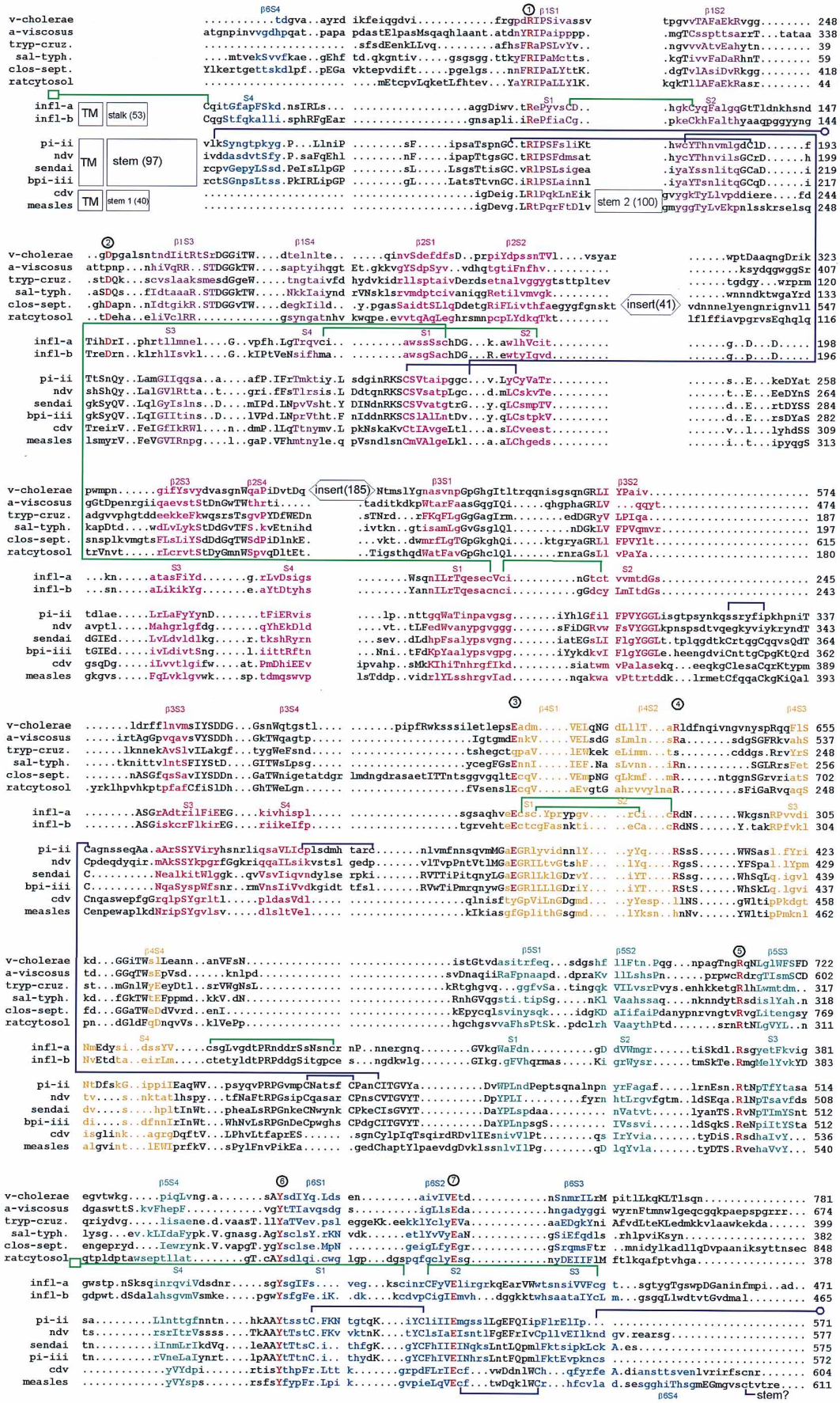
v-cholerae
a-viscosus
tryp-cruz.
sal-typh.
clos-sept.
ratcytosol
infl-a
infl-b
pi-ii
ndv
sendai
bpi-iii
cdv
measles
TM
stalk (53)
stem (97)
stem 1 (40)
stem 2 (100)
insert(41)
insert(185)
stem?

TABLE 1. Similarities between neuraminidases and transneuraminidases of bacterial, protozoan, viral, or eukaryotic origin

Protein type	Similarity[a]													
	V. cholerae	*A. viscosus*	*T. cruzi*	*S. typhimurium*	*C. septicum*	Rat cytosolic	Influenza virus A	Influenza virus B	PIV-2	NDV	Sendai virus	PIV-3	CDV	Measles virus
V. cholerae		59	53	61	77	54	34	29	30	30	30	33	15	21
A. viscosus	59		48	69	77	51	33	28	25	26	30	28	26	20
T. cruzi	53	48		78	59	48	31	37	26	31	32	34	30	26
S. typhimurium	61	69	78		94	56	30	31	33	33	33	27	25	27
C. septicum	77	77	59	94		64	42	29	30	23	32	31	29	24
Rat cytosolic	54	51	48	56	64		23	25	31	31	21	25	25	24
Influenza virus A	34	33	31	30	42	23		112	35	32	31	27	24	25
Influenza virus B	29	28	37	31	29	25	112		38	29	28	27	25	23
PIV-2	30	25	26	33	30	31	35	38		151	105	107	38	36
NDV	30	26	31	33	23	31	32	29	151		114	103	33	41
Sendai virus	30	30	32	33	32	21	31	28	105	114		233	46	44
PIV-3	33	28	34	27	31	25	27	27	107	103	233		50	51
CDV	15	26	30	25	29	25	24	25	38	33	46	50		135
Measles virus	21	20	26	27	24	24	25	23	36	41	44	51	135	

[a] Each comparison gives the number of identical residues according to the alignment of Fig. 1.

aminidase. Correspondingly, the primary sequences of paramyxovirus HN and influenza virus N also have a low similarity (7.1 to 10%) (Table 1), but Colman et al. (9) proposed very convincingly that HN may adopt the same fold. The similarity between influenza virus N and morbillivirus H is even lower (6.3%), but the similarity between paramyxovirus HN and morbillivirus H is higher (11.4 to 14.5%) than the similarity of paramyxovirus HN with influenza virus N (7.1 to 10%) (Table 1). Therefore, the parainfluenza virus sequences can be used as an intermediate to align the morbillivirus H with the influenza virus N sequences. Because the structural model of parainfluenza virus HN is used as an intermediate to build the model of measles virus H, the greatest uncertainty of the model is the similarity between influenza virus N and parainfluenza virus HN. The first part of the alignment of morbillivirus H with other neuraminidases or transneuraminidases is complex, especially the alignment of the first sheet and the location of the second stem region. According to alignment procedures described in Materials and Methods, a global homology is found approximately C terminally from position 226. However, the highest, most significant local homology was found for L105-R106-T107-P108, which is homologous to the most conserved region in all neuraminidases and transneuraminidases. To incorporate this best local homology with great functional importance with the best global alignment, an excessive gap had to be introduced in the morbillivirus H sequence alignment. As a result, a major part corresponding to the possible parainfluenza virus stem region is deleted from the alignment, and a large part is inserted in β1L12 (Fig. 1). A possible topology of morbillivirus H is as follows: after the transmembrane region, the first, smaller stem insert extends up to the neuraminidase head; the large, second insert appears in a loop of the neuraminidase β-propeller, which suggests that right after the first β-strand of the β-propeller, which contains the very important first catalytic arginine, the polypeptide folds back under the neuraminidase head to form a stem together with the smaller insert, and then the chain returns to continue the β-propeller (Fig. 2). The relatively large deletions in sheets β5 and β6 typical for morbillivirus H may be a consequence of the bulky stem region of morbillivirus H, and perhaps Cys606 is connected to a cysteine in the stem.

By using the alignment (Fig. 1), a 3D model of a paramyxovirus HN was constructed by replacing the residues of the crystal structure of influenza virus N with the homologous residues of bPIV-3 (Fig. 3a). For residues contained in gap regions according to the alignment, loop searches were performed as described in Materials and Methods. The large loops that were constructed in this way have an especially high uncertainty. The loops were chosen from a group of loops which were selected on the basis of homology and distance of the anchor residues in the start and the end of the loop. The final choice is arbitrary and was based on structural limitations in the 3D space of neighboring loops, positioning of important residues in the active site, or close spatial positioning of cysteine residues which likely form a disulfide bridge. Finally, the structure was minimized. Similarly, a 3D model of measles virus H was built (Fig. 3b) according to the alignment of bPIV-3 HN and measles virus H (Fig. 1) as described above. The modelled 3D structure of bPIV-3 HN was used as a framework for the homology modelling of measles virus H.

Locations of insertions and deletions in *Paramyxoviridae* HN and H. The reliability of the model is strengthened when insertions and deletions occur at appropriate locations. According to the alignment (Fig. 1) and the model (Fig. 3a and b), the large insertions (β1L01, β2L01, β2L23, β3L01, β5L01, and β5L12) and the very large insertions (β3L23 and β4L01) are all located on the top of the barrel, except for β5L12. This is in accordance with the general neuraminidase fold, in which the top loops (L01 and L23) are always extensive compared with the bottom loops (L12 and L34). In contrast, the large deletions (β1L23, β5L01, β5L34, and β6L12) seem equally distributed over the top or bottom of the barrel. The bottom deletions are found in the C-terminal part of the barrel in sheets β5 and β6 and are larger for morbilliviruses than for other viruses.

The alignment in Fig. 1 is constructed from four groups of different multiple sequence alignments which display a low homology between the groups (Table 1). Reliable alignments display a high homology and few gaps. Because the number and length of gaps affect the quality of an alignment, the

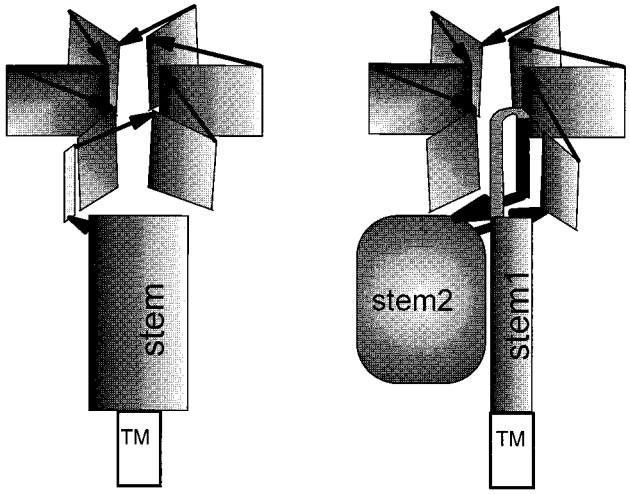

FIG. 2. Diagram of global structures of paramyxovirus HN (a) and morbillivirus H (b). The top section indicates the β-propeller in which the six sheets are shown as rectangles. Stem and transmembrane (TM) regions and the direction of the polypeptide chain (arrows) are indicated.

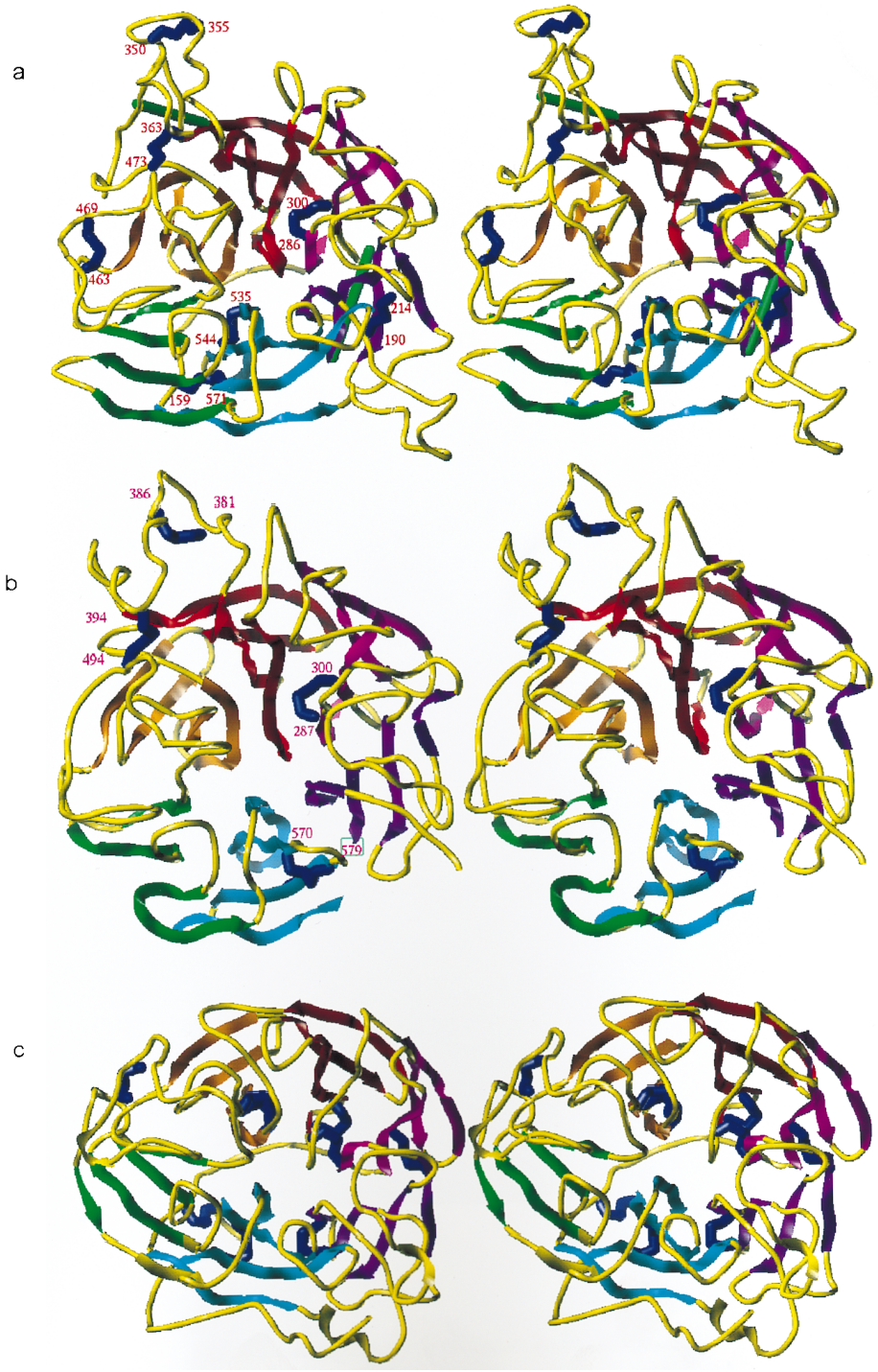

FIG. 3. (a) Stereo ribbon diagram showing the hypothetical folding of bPIV-3 HN. β-Sheets are color coded as indicated for Fig. 1. Probable cystine bridges are shown in blue for bPIV-3 and in green for additional cystine bridges in other paramyxoviruses. Cys159-Cys571 connects the N terminus of the model with β6S3, and Cys190-Cys214 connects β1L01 with β1L23. Cys204-Cys265 connects β1S2 with β2L12 of mumps virus, NDV, SV-5, and PIV-2; Cys256-Cys269 connects β2S1 with β2S2; Cys350-Cys355 lies within β3L23 of PIV-3 and Sendai virus; Cys363-Cys473 connects β3L23 with β5L01; Cys384-Cys394 connects β3S4 with β4L01 of mumps virus, SV-5, and PIV-2; Cys463-Cys469 lies within β5L01; and Cys535-Cys544 connects β6S1 with β6S2. Residue numbers are only shown in the left part of the stereo picture. (b) Hypothetical model for measles virus H. Cys287-Cys300 connects β2S1 with β2S2, Cys381-Cys386 lies within β3L23, Cys394-Cys494 connects β3L23 with β5L01, and Cys570-Cys579 connects β6S2 with β6S3. (c) Crystal structure of influenza virus N (56). Views are from above the active site.

introduction of gaps in an alignment is not favorable. However, the similar locations of some gaps in independently aligned groups of the total alignment (Fig. 1) reinforce the quality of the alignment. Thus, some of the insertions introduced in the alignment of influenza virus N with *paramyxoviridae* HN/H are more acceptable because they appear in regions which also show gaps in another group of the total alignment (Fig. 1). For example, an insertion is present in β1L01 of paramyxovirus

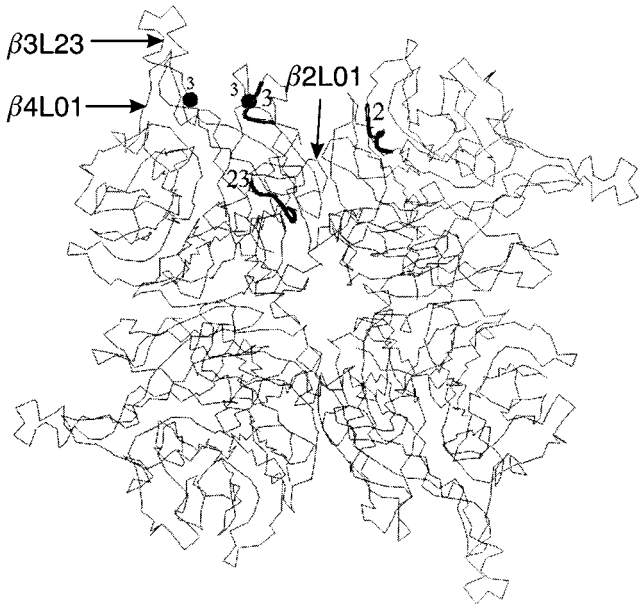

FIG. 4. Hypothetical model of bPIV3 HN tetramer. Antigenic sites 2, 3, and 23 (tubes) and escape mutations on antigenic site 3 (spheres) are indicated. The large insertions β3L23 and β4L01 are shown.

HN, and a much larger insertion is present in β1L01 of bacterial-protozoan N. Similar insertions or deletions present in *Paramyxoviridae* HN or H and in bacterial-protozoan N occur in β1L23, β2L01, β2L23, β3L01, and β4L01.

Disulfide bridges. According to the 3D structure of bPIV-3 HN and measles virus H, cystine bridge pairing can be detected (Fig. 3a and b). Strikingly, there is no single conserved cysteine bridge between influenza virus N and *Paramyxoviridae* HN or H (Fig. 1 and 3). One exception may be a cystine bridge between β6S2 and β6S3 in influenza virus N and morbillivirus H, but even this bridge is not structurally similar because in N the start of S2 is connected to the end of S3, whereas in H the end of S2 is connected to the start of S3.

All cystine bridges in the morbillivirus model are conserved compared to the cystine bridges in parainfluenza virus HN, except for the cystine bridge between β6S2 and β6S3 in morbillivirus H.

Cystine bridges between residues 159 and 571, 190 and 214, 204 and 265, and 535 and 544 in parainfluenza virus HN were previously predicted by Colman et al. (9).

A study of the role of the individual cysteine residues in the HN protein of NDV (40) suggested that (according to bPIV-3 numbering) cysteines 190 and 214 are linked; cysteines 204, 256, 265, and 269 are linked in some way; cysteines 363, 463, 469, and 473 are linked in some way; and cysteines 535 and 544 are linked. These results agree with our model if bPIV-3 and NDV show identical cystine bridge connections.

Tetramer interface. The HN and H proteins are thought to form tetramers as mature proteins (8, 37, 41, 44, 55). A model of the tetramer was generated by superimposing the monomer models on the backbone of the influenza virus neuraminidase tetramer (Fig. 4). The two largest insertions (>15 residues) are located on β3L23 and β4L01, which agrees with the tetramer model, because these loops are on the outside of the tetramer, away from the interfaces. The only region that seems to obstruct an appropriate tetramer formation is the inserted β2L01 loop. Therefore, in the actual structure, β2L01 must be located more towards the active site. Most conserved noncharged residues in measles virus H are located on β-sheets 1 and 2, which form part of the tetramer interface.

Glycosylation sites. The potential glycosylation sites in the model of bPIV-3 HN are located on the surface and mostly on loops on the top of the molecule. For bPIV-3 HN, the potential glycosylation sites are located on β3L01, β3L23, β5L01, β6L01, β6S3, and β6S4 (Fig. 5, top, in purple). β6L01, β6S3, and β6S4 cluster in the 3D space. However, β6S3 is less likely to be used because a carbohydrate at this site may obstruct tetramer formation. Two potential paramyxovirus glycosylation sites that have no direct counterpart in bPIV-3 reside on β4L01 (mumps virus and PIV-2) and β5L23 (Sendai virus, PIV-2, and mumps virus) (Fig. 5, top, in yellow). The first is very close to the potential glycosylation site on β5L01 of bPIV-3, and the second is very close to the potential glycosylation site on β6L01 of bPIV-3. β3L01 is very close to an N-linked carbohydrate in the structure of influenza virus A neuraminidase on β2L23. Strikingly, most potential glycosylation sites are located away from the tetramer interface. For NDV HN, the actual usage of sites has been determined (39). Sites 2 (β3L23), 3 (β4S4), and 4 (β5S2) can be accommodated in the structure and are located at the side or bottom of the tetramer, away from the tetramer interface. Site 5 (β5L23) is hidden in the interior and is located right under an active-site residue. A glycosylated site 6 (β6L12) might interfere with tetramer formation. This might explain why potential glycosylation sites 5 and 6 are not used (39).

For measles virus, most potential glycosylation sites are located on the postulated stem region. Only one potential glycosylation site, which is not used in this strain (21), is located on the neuraminidase head, on loop β1L23 (Fig. 5, middle, in purple). The corresponding loop in influenza virus A and B neuraminidase contains the only conserved glycosylation site. Three potential morbillivirus glycosylation sites on H that have no counterpart in measles virus reside on β3L23 (RPV and PDV), β4L01 (PDV and CDV), and β6S4 (PDV and CDV) (Fig. 5, middle, in yellow), all of which have counterparts in paramyxovirus HN.

Epitopes. The bPIV-3 HN model can be used as a general model for paramyxovirus HN. Therefore, antigenic sites of all HN proteins can be used for localizing the epitopes on the 3D model of bPIV-3 HN. Loop β1L23 corresponds to antigenic site 23 in NDV HN, as described by Iorio et al. (24). Antibodies against antigenic site 23 recognize only the oligomer (38), which agrees with the location of β1L23, which is close to the tetramer interface (Fig. 4). NDV-HN antigenic site 23 is very close to antigenic sites 2 (β5) and 3 (β2L23, β3S4, and β3L23), which is in agreement with competition studies (25). Overlap with site 3 is probably an intramonomer overlap, and overlap with site 5 is probably an intermonomer overlap (Fig. 4).

Antibody escape mutants with substitutions at residue positions 363 and 472 of SV-5 were selected by antibodies directed against antigenic site 4 (2). According to the alignment, the mutations are located on β3L23 and β5L01 next to a postulated disulfide bridge, corresponding to the bPIV-3 HN model. The vicinity of both mutations within the discontinuous epitope agrees with the tertiary structure of the HN model. Substitutions disrupting the binding of antibody directed against antigenic site 5 of SV-5 HN occur at positions 453, 498, and 541. In the model, these residue positions are located on β5L01, β5L23, and β6L12, respectively. Residues 453 and 498 of SV-5 are located on top of the molecule on two neighboring loops according to the bPIV-3 model (Cα atoms within 11 Å). However, residue 541 of SV-5 is located on the bottom of the molecule. It is possible that the model is incorrect at this point.

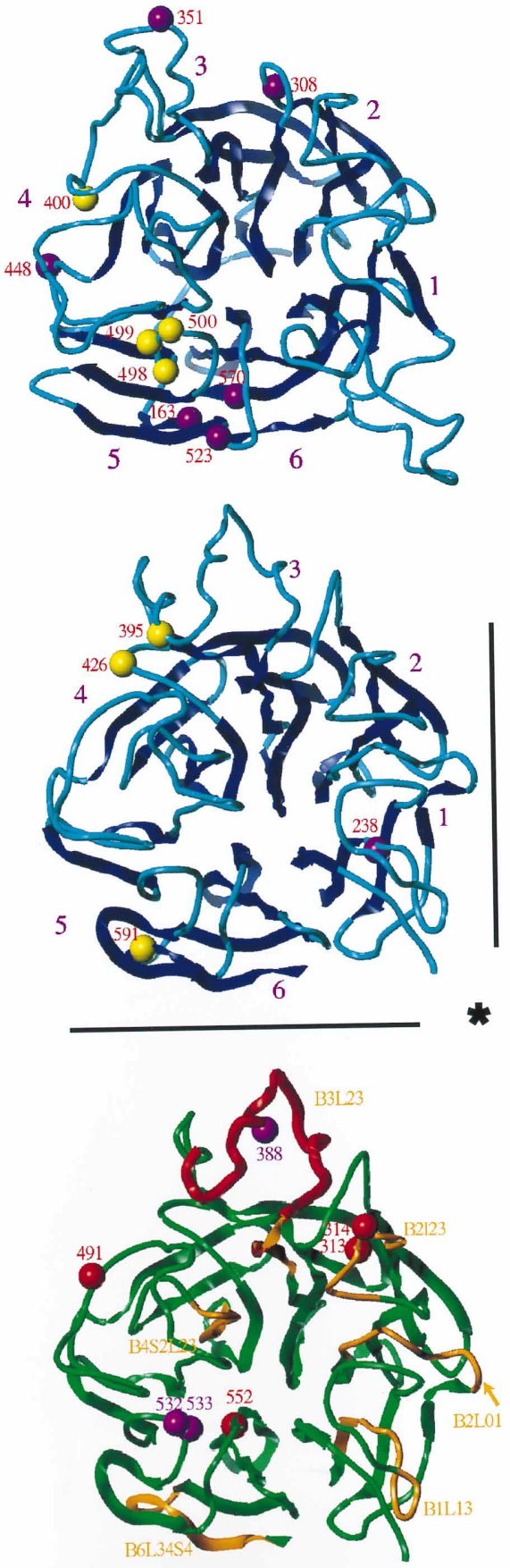

Otherwise, antigenic site 5 may map to the side of the molecule and span from the top to the bottom of the molecule. Alternatively, a mutation which structurally compensates for a harmful mutation may itself lie outside the antigenic site recognized by the selecting monoclonal antibody (MAb).

In human PIV-3 HN, mutation of residue 281 or 370 and of residue 278 disrupts binding of antibodies against overlapping epitopes I and VI, respectively (6). Residues 278 and 281 are located on the exposed surface loop β2L23. However, proline 370 is located 30 Å away on β3S3 and is not exposed. Perhaps mutation of residue 370 can allosterically induce a conformational effect on the epitope.

Because the antigenic regions of measles virus H protein have been studied extensively, these data are very useful for checking the validity of the measles virus H model. Comparison of the location in the 3D model of epitopes mapped with the aid of short synthetic peptides (35, 36) showed that antigenic sites are located on β1L23, β2L01, β2L23, and β3L23 on the top of the molecule and β4S2L23 and β6L34S4 (Fig. 5, bottom, orange). All of these regions except for β4S2L23 are in agreement with the model because they are exposed on the protein surface.

With the aid of five MAbs, four antigenic sites on measles virus H protein could be characterized (20, 53). For these mAbs (MAb I-29 to site I, MAb 16-CD11 to site II, MAbs 16-DE6 and I-41 to site III, and MAb I-44 to site IV), the epitopes were determined by sequencing selected MAb-resistant mutants. MAb I-29 maps to residues 313 and 314 on a large insertion on top of β2L23 (Fig. 5, bottom, red). This epitope was also mapped with peptide binding studies (35, 36). MAb I-41 maps to residue F552 (Fig. 5, bottom, red), the first residue on strand β6S1 in the center of the molecule right under active site residue Y551. MAb 16-CD11 maps to residue 491 at the center of the large loop β5L01 (Fig. 5, bottom, red). MAb 16-DE6 mapped to residues 211, 388, 532, and 533 (20). Because residue 211 lies outside the model somewhere between β1S1 and β1S2, the spatial relationship with other residues in the same antigenic site cannot be verified with the 3D model. Residue 388 and residues 532 and 533 are located on top of the molecule on loops β3L23 and β5L23, respectively (Fig. 5, bottom, purple), and therefore this discontinuous antigenic site supports the model. According to Liebert et al.(33), the major antigenic site of measles virus H protein is located between residues 368 and 396, which corresponds exactly to the large insertion at β3L23.

Active site. (i) Paramyxovirus. The alignment (Fig. 1) predicts that six of the seven common active-site residues are

FIG. 5. (Top) Locations of potential glycosylation sites in hypothetical model of bPIV-3 HN (shown as purple spheres at positions 308 on β3L01, 351 on β3L23, 448 on β5L01, 523 on β6L01, 570 on β6S3, and 163 on β6S4) and locations of potential glycosylation sites in mumps virus or Sendai virus HN, which are not conserved in bPIV-3 HN (shown as yellow spheres in the corresponding positions of bPIV-3 HN at residues 400 in β4L01 and 498, 499, and 500 in β5L23). Sheets (blue and indicated with numbers) and loops (cyan) are indicated. (Middle) Location of potential glycosylation site in model of measles virus H (shown as a purple sphere at position 238 in loop β1L23) and locations of potential glycosylation sites in RPV, PDV, and CDV H which have no counterpart in measles virus H (shown as yellow spheres in the corresponding positions of measles virus H, at residues 395 on β3L23, 426 on β4L01, and 591 on β6S4). Sheets (blue, with numbers) and loops (cyan), interfaces with other H monomers (lines), and the center of the tetramer (asterisk) are indicated. (Bottom) Epitopes on measles virus H. Linear antigenic sites (235 to 245, 276 to 285, 309 to 318, 368 to 377, 442 to 451, and 587 to 596) according to peptide binding studies are colored cyan (35, 36). Antibody escape mutations (residues 313, 314, 491, and 552) of several antibodies (pink spheres), antibody escape mutations (residues 388, 532, and 533) of MAb 16-DE6 (20) (red spheres), and a major antigenic region (33) (red thick tube) are shown.

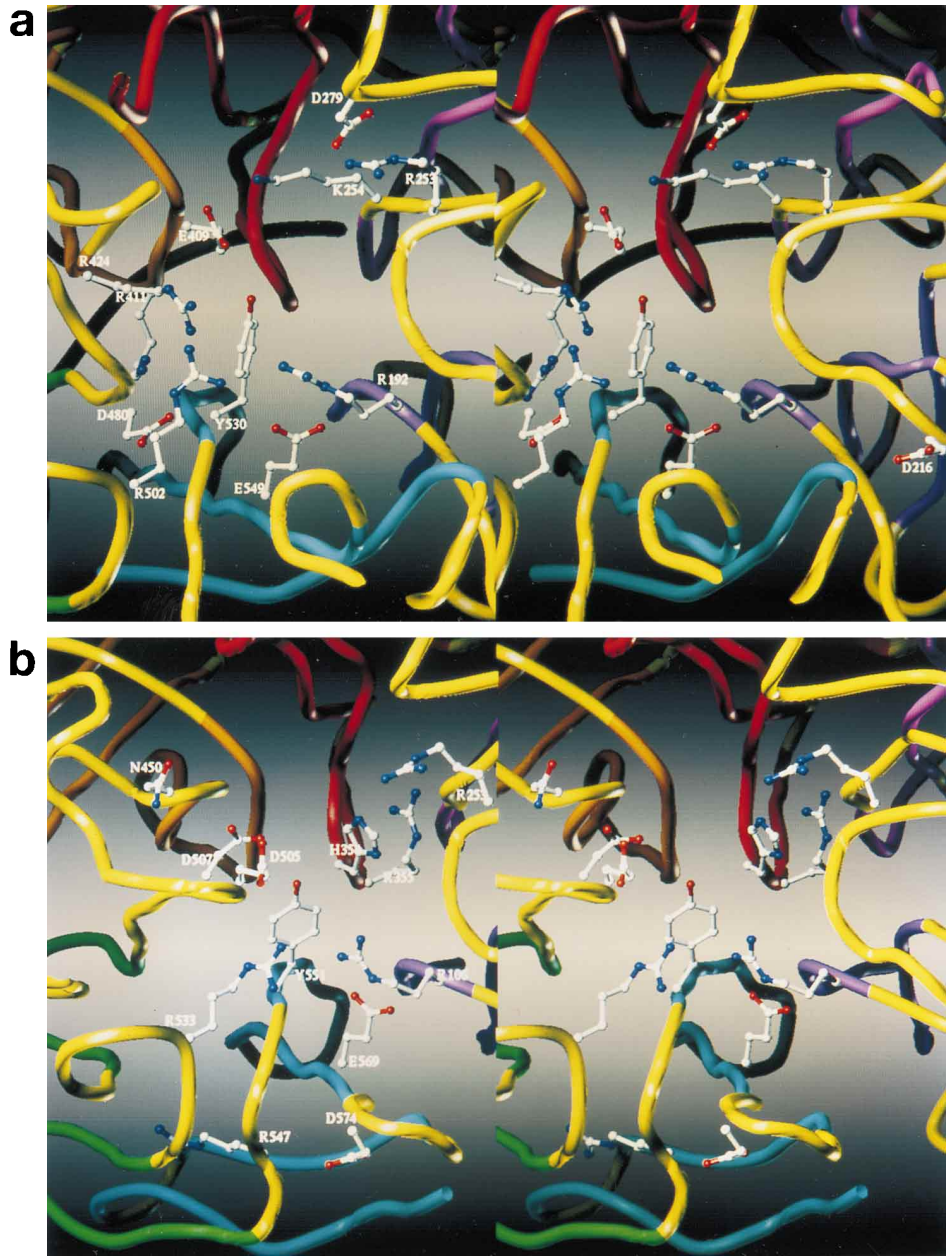

FIG. 6. (a) Stereoviews of active site in hypothetical models of bPIV-3 HN (a) and measles virus H (b). Both sites are viewed from above the active site. Color coding of secondary structures is as for Fig. 1 and 3.

conserved in paramyxovirus HN (Fig. 6a). The active-site influenza virus residue D151 has no homolog in paramyxovirus HN according to the alignment. Influenza virus residue D151 is probably involved in proton transfer; however, the enzyme is active above the pK_a of D151. Therefore, a nonspecific proton donor, such as a water molecule, may be involved (4). Influenza virus D151 aligns with parainfluenza virus Q222, but Q cannot act as the proton donor. As mentioned above, the role of influenza virus D151 is still obscure; the conservation in influenza virus and some bacterial neuraminidases suggests an important function, but according to the sequence alignment the aspartic acid is also not conserved in *Streptomyces lividans* (*M. viridifaciens*) and *A. viscosus*. If an aspartic acid is the proton donor, then two candidate residues can be conceived: parainfluenza virus D216 in β1L23 or parainfluenza virus D279 in β2L23. In the case of parainfluenza virus D216, the alignment needs minor justification; in the case of parainfluenza virus D279, loop β2L23 has to be remodelled for the correct orientation of D279 in the active site.

The most conserved region of paramyxovirus HN corresponds to the ^{252}NRKSCS^{257} sequence located on β1L01-β2S1. The region corresponds to the only sheet in influenza virus that does not contain active-site residues. Parainfluenza virus residue R253, which is part of the highly conserved stretch NRKSCS, may be homologous to the conserved influenza virus R152. In that case, parainfluenza virus R253 is not homologous to influenza virus R224 as suggested by Colman et al. (9), but instead the positively charged parainfluenza virus

residue K254 may be homologous to influenza virus R224. Influenza virus R152 has an important active-site structural role because it directly contacts *N*-acetyl of sialic acid, while influenza virus R224 is just a framework residue which holds influenza virus E276 in place. Because there is no homolog for influenza virus E276 in HN, such a framework function is not expected in parainfluenza virus HN. Perhaps parainfluenza virus K254 holds active-site residue E409 in place (Fig. 6a).

Parainfluenza virus residues R411 and D480 are conserved charged residues, close to active-site residue Y530, without counterparts in influenza virus N. Perhaps parainfluenza virus R411 is a framework residue for active-site residue parainfluenza virus E409 or it may contact parainfluenza virus D480. As suggested by Colman et al. (9), parainfluenza virus D480 may be a framework residue that binds parainfluenza virus R424 (fourth active-site residue).

(ii) Morbillivirus. After close inspection of the location of all conserved charged residues in the 3D model of MV H, we noticed that most conserved charged residues are clustered at the top center of the β-propeller, where the active site is located in neuraminidases. The clustering of conserved charged residues is suggestive for a conserved glycosidase activity in measles virus H. The highest conservation was observed for amino acids that are close to the glycoside bond of sialic acid. Although for H of morbilliviruses only hemagglutination and no neuraminidase activity has been reported, some conserved active-site residues suggest that H has enzymatic activity.

The alignment (Fig. 1) predicts that four of the seven common active-site residues, as described in the introduction, are conserved in morbillivirus H. Measles virus residue R106 is homologous to influenza virus R118, measles virus R533 is homologous to influenza virus R371, measles virus Y551 is homologous to influenza virus Y406, and measles virus E569 is homologous to influenza virus E425 (Fig. 6b). The conservation of both measles virus residues R106 and E569 is coherent because these two residues form a conserved couple important for the catalytic mechanism of neuraminidases (4). According to the alignment, the conserved measles virus residue R533 has a very important role in substrate binding: it binds the acidic group of sialic acid and is responsible for the precise orientation of the sugar for the glycosidic cleavage. Measles virus residue Y551 is one of the most important residues in the reaction mechanism because it stabilizes the oxocarbonium intermediate. Furthermore, two additional active-site residues are conserved: measles virus R253 is homologous to influenza virus R152, and measles virus N450 is homologous to influenza virus N294.

In general, no homologies are observed for the side of the active site that interacts with the sialic acid glycerol side chain in influenza virus neuraminidase.

According to the alignment (Fig. 1) there are no homologs in morbillivirus H for the typical active-site residues 2, 3, and 4 corresponding to influenza virus residues D151, E277, and R291, respectively. According to the alignment, active-site residue 2 is also not present in the neuraminidases of paramyxovirus, *Streptomyces lividans*, or *Actinomyces viscosus*. Active-site residues 3 and 4 are also not present in the neuraminidase of *T. cruzi* listed in Fig. 1. In contrast to the alignment between paramyxovirus HN and influenza virus N, the missing aspartic acid of active-site residue 2 cannot be solved by a justification of the alignment. The third active-site residue of influenza virus E277 on β4S1, which is missing in morbillivirus H, has an important role in the neuraminidase mechanism of influenza virus because it accepts a proton from influenza virus active-site residue Y405. In the 3D space, this active-site residue may be substituted by another proton acceptor. The negatively charged conserved residues D505 and D507 are located on an insertion on loop β5L01. The important location and conservation suggest a possible role for these residues in the active site. There are no obvious homologs for these residues in other neuraminidases according to the alignment, but maybe D505 or D507 substitutes for the missing active-site residue corresponding to influenza virus E277 and the framework residue corresponding to parainfluenza virus D480.

One of the few candidates for the missing fourth active-site residue (influenza virus R292 on β4S2) is measles virus R547 on β6L01. However, the 3D model does not support a superposition of influenza virus R292 and measles virus R547.

A remarkable conserved cluster of residues in morbillivirus H consists of Q109 on β1S1 and H354 and R355 on a characteristic β-bulge on β3S1. The residues are close to the ligand binding site. The residues approximate the 3D space occupied by conserved negatively charged residues in β2S1 or β3S1 in bacterial and influenza virus neuraminidases, respectively. The role of the residues is unknown, but their location and conservation suggest a possible role in proton transfer. Several conserved negatively charged residues are found near the ligand binding site of measles virus: measles virus residues E256, D530, and D574 on β1L23, β5L23, and β6L23, respectively but none of these are superimposable on influenza virus D151.

G432, P433, and I435 are conserved noncharged residues on β4S1 at the bottom of the active site. These residues are very close to P368 on β3S2, which also lines the active-site pocket. On the other side of the active site, the conserved residues G104, L105, P108, and Q109 on β1L01 and β1S1 line the pocket.

Neuraminidase assays. Because the 3D model of morbillivirus H suggested a neuraminidase activity that has never been described before, neuraminidase assays were performed with RPV and a large selection of neuraminidase substrates (Fig. 7). Sialic acid was released only from mucin type 1, isolated from bovine submaxillary glands. Figure 8 shows that the neuraminidase activity of RPV was dose dependent and that no activity was found in supernatants of mock-infected or BRSV-infected cells. Next, measles virus, PDV, CDV, DMV, and PPRV were tested for neuraminidase activity. Only PPRV showed a low neuraminidase activity, only with bovine submaxillary mucin type 1 (Fig. 8). Neuraminidase from *C. perfringens* showed good activity with mucin type 1 (data not shown), but bPIV-3 did not. Neuraminidase activity of RPV could be inhibited to 2.9% by preincubation of RPV with an RPV-specific polyclonal cow serum.

The optimal pH for the RPV-associated neuraminidase is shown in Fig. 9. The activity of RPV neuraminidase extends over a relatively wide and acidic pH range, with an optimum between pH 4 and 5, which is typical for viral neuraminidases.

Neuraminidase activity was reduced to 50% after incubation of the virus at 61°C for 25 min, and neuraminidase was completely inactivated after heating at 100°C for 2 min. Activity could not be inhibited by the *N*-acylneuraminidase inhibitor DANA (2,3-dehydro-2-deoxy-*N*-acetyl-neuraminic acid). Like paramyxovirus HN, the neuraminidase activity of RPV was independent of calcium (data not shown).

Hemadsorption assay. At 20°C, *Cercopithecus* erythrocytes adsorbed in a single cell circle around spots showing cytopathic effect of a measles virus-infected monolayer. After incubation at 37°C for 3 h, in order to activate the presumed neuraminidase activity, all adsorbed erythrocytes were detached from the monolayer. Subsequently, the infected cells were still able to adsorb erythrocytes at 20°C.

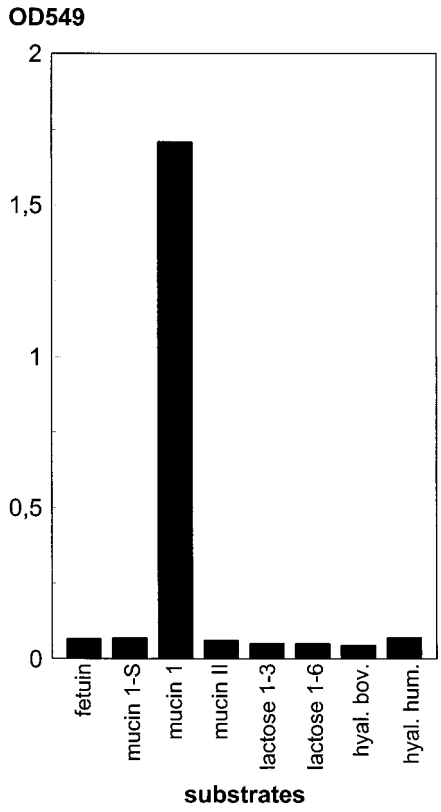

FIG. 7. Neuraminidase activity in RPV determined by using different substrates. RPV was sedimented by ultracentrifugation. A total of 4.6 50% tissue culture infective doses of RPV in 50 μl was incubated overnight at 37°C with the substrates as described in Materials and Methods. OD549, optical density at 549 nm; hyal. bov. and hyal. hum., bovine and human hyaluronic acid, respectively.

DISCUSSION

In this study, 3D structures are proposed for the attachment proteins of all *Paramyxovirinae* and *Morbillivirinae*. The structure of influenza virus N was used as a framework for modelling the paramyxovirus HN, extending a previous proposal for the gross structural arrangement of this protein (9, 26). The neuraminidase multiple sequence alignment could be extended with morbillivirus H sequences when the paramyxovirus HN sequences were used as an intermediate. Consequently, a 3D structure of morbillivirus H could be modelled on the parainfluenza virus HN framework.

Most insertions in the larger neuraminidase heads of paramyxoviruses are located in loops at the top surface of the molecule. This is in accordance with the general neuraminidase fold, in which the top loops are always extensive and more variable compared with the bottom loops. Additionally, most published experimental data agreed with the 3D model. Most epitopes are located on the top loops of the paramyxovirus heads. Multiple mutations in discontinuous epitopes, which were scattered over a large part of the primary sequence, were close in the 3D model. The large insertions are located at sites that are not in the interface of the possible tetramerization sites of the molecule. The potential glycosylation sites were located mostly at the molecular surface, and some sites had counterparts in the influenza virus neuraminidase molecule. Although the cysteine residues were not conserved in the alignment, all residues could be paired in cystine bridges, which is a strong support for the 3D model. Finally, the spatial arrangements of proposed active-site residues are similar to those of the active-site residues seen in other neuraminidases of known structure. Moreover, the model implies which additional, hitherto-unrecognized residues are important for neuraminidase activity or active-site structure. For measles virus H, this predicts hitherto-undescribed enzymatic activity. The prediction embarked a search for the right substrate to prove glycosidic activity in a morbillivirus. Eventually, neuraminidase activity was found for RPV and PPRV with mucin isolated from bovine submaxillary glands. Furthermore, the temperature-dependent hemadsorption of measles virus suggests that this virus also has neuraminidase activity.

The alignment of paramyxovirus HN differs from the approximate alignment described by Colman et al. (9) in only one region. They proposed an insertion in HN corresponding to sheet 3 of influenza N, and the start of sheet 3 differs by about half the length of the sheet compared to the alignment described in this study. Because of the higher homology between *paramyxoviridae* HN and H sequences, alignment of HN and H was more easily compared with the alignment of these proteins with other neuraminidases. In general, the structures of the loop regions especially are ambiguous. Both models should be taken as approximate, and future evidence may improve the accuracy of the models.

The models illustrate the diverse solutions for the elevation of a neuraminidase head above the viral membrane. In the case of influenza virus, the neuraminidase head is extended above the membrane by a stalk region of approximately 40 amino acids. The stalk lifts the neuraminidase head to approximately the same height as the other viral membrane protein, the hemagglutinin, which contains membrane fusion activity. There is no indication for a stalk region in the *Paramyxovirus* or *Morbillivirus*. However, the corresponding region in paramyxovirus HN, between the transmembrane region and the neuraminidase head, contains a large protein domain (between residues 56 and 161) which has high alpha-helix propensity, according to neural-network-based secondary-structure predictions (data not shown). It is likely that this is a helical stem region that supports the neuraminidase head and lifts it to the same height as the fusion protein, comparable to the case for

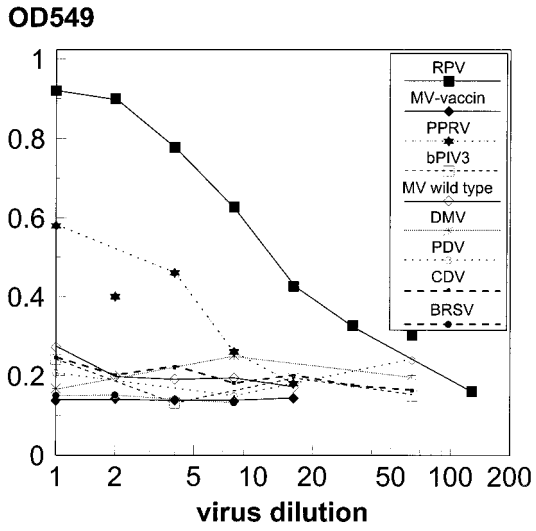

FIG. 8. Dose-response curves of different morbillivirus dilutions, bPIV-3, and BRSV. The concentration of virus (*x* axis) is plotted against the amount of sialic acid released from mucin 1 (*y* axis). OD549, optical density at 549 nm; MV, measles virus.

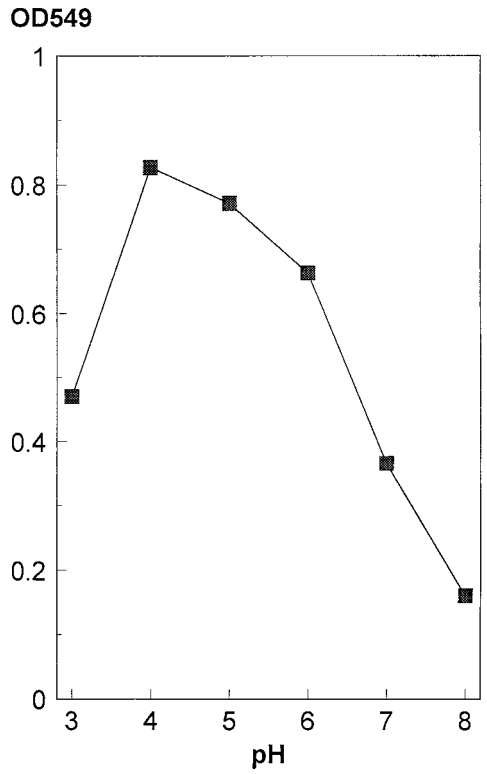

FIG. 9. Neuraminidase pH optima. The neuraminidase activity of 4.5 50% tissue culture infective doses of RPV was assayed under various pH conditions. OD549, optical density at 549 nm.

influenza virus. According to the unusual alignment, morbilliviruses have acquired a completely different helix-rich domain which is made up of two insertions (a 40-residue insert between residues 58 and 98 and a 110-residue insert between residues 115 and 225, Fig. 1), the larger of which is located inside the neuraminidase head domain instead of N-terminal to the neuraminidase head as observed in influenza virus and paramyxovirus (Fig. 2). Although the two-insert scenario in morbillivirus H is not elegant, it is the only way to combine the highest local and the highest global similarities in the alignment. Analogous to the stem region of paramyxovirus HN, both stem region insertions of morbillivirus H also have high helix propensity according to neural-network-based secondary-structure predictions. Excessive insertion within a neuraminidase gene is not unique. Within the *V. cholerae* neuraminidase, an insertion of a lectin domain of 193 residues has occurred (10) in β3L01, between sheets 2 and 3.

Apart from the stem region, the most excessive insertion in *Paramyxoviridae* HN/H is the 28- to 36-residue-long insertion in β3L23. This region is the most immunodominant region of measles virus H. The presence of this large insertion in all *Paramyxoviridae* HN or H proteins compared with influenza virus or bacterial or protozoan N proteins, the lack of any active-site residues in the loop and the antigenicity of the loop support a possible role as a surface-exposed receptor binding site for β3L23. Interestingly, for measles virus, this region is a neutralization site (59) and may play a role in the neurovirulence of the virus (33). Measles virus H and some paramyxovirus HN proteins contain a cystine noose in β3L23 between Cys381 and Cys386. Such nooses are often involved in protein-protein interaction (30). According to Ziegler et al. (59), a cystine noose is present between Cys386 and Cys394. In that case, the structurally ill-defined loop should be remodelled to allow a residue 386-394 and a residue 381-494 pairing. Functional studies with chimeric measles virus H protein showed that residues 491, 493, 495, 505, and 506 may be involved in agglutination to erythrocytes because these mutations abrogated binding of a MAb directed to a nonagglutinating H protein (23). Shibahara et al. (54) showed that residue 546 is involved in agglutination. These studies suggest that the adjacent loops β5L01 and β6L01 are involved in binding activity of measles virus H. It is presumed that measles virus H binds erythrocytes through CD46 (15, 43). However, freshly isolated wild-type strains do not interact with CD46 (32). This suggests that wild-type measles virus uses a different receptor to initiate infection (32). Use of multiple receptors has previously been described for human immunodeficiency virus type 1 (17) and may likely be general in virus infections. At least three ligands for H may play a role during infection: sialic acid via the center of the β-propeller during transport through the mucus layer, CD46 via β5L01 and β6L01 for attachment to cells, and additionally a possible interaction with F via an unknown site.

The neuraminidase gene is probably spread from eukaryotic cells by horizontal gene transfer among bacteria, fungi, and protozoa during association with their animal hosts (50). It is not known whether viral neuraminidase genes also have a eukaryotic origin. A recently cloned eukaryotic neuraminidase gene for rat cytosolic neuraminidase has a very weak homology with bacterial and protozoan neuraminidases (42) (Fig. 1). Maybe new eukaryotic sequences will bridge the distances between the neuraminidase superfamily members. In contrast to bacterial and protozoan neuraminidases, viral neuraminidases are transmembrane proteins and they are organized as tetramers. The viral proteins do not possess the Asp-box motif (Ser/Thr-Xaa-Asp-[Xaa]-Gly-Xaa-Thr-Trp/Phe), and especially the influenza virus and paramyxovirus neuraminidases contain more cystine bridges than bacterial and protozoan neuraminidases. Perhaps the viral neuraminidases are examples of unique convergent evolution, but if the neuraminidase gene is transferred from a higher organism to the virus, then several evolutionary scenarios are possible for an archetypal myxovirus. It is possible that the archevirus may have possessed an attachment protein that was lost, or changed radically, after the introduction of the neuraminidase gene. Alternatively, the archevirus possessed just one membrane protein, the fusion protein. For its proper function, the introduced neuraminidase acquired several characteristics as mentioned above: a transmembrane region and a tetrameric organization, cystine bridges, and an extension of the neuraminidase head to lift it to the same height as the other membrane protein with which it evolved a probable cooperation as is shown for some of the *Paramyxoviridae* (3, 5, 13, 22, 52). On the basis of the low overall amino acid homology between influenza virus N and *Paramyxoviridae* HN and H, and especially the divergence in cystine bridge connection, it is likely that influenza virus and *Paramyxoviridae* neuraminidases are not evolutionary related. Additionally, because the gene is not present in viruses which are more evolutionarily related to influenza virus or the *Paramyxoviridae*, the neuraminidase gene in orthomyxovirus, influenza virus, and the *Paramyxoviridae* may be introduced independently. Morbillivirus H contains very few cystine bridges, but most of these cystine bridges are conserved with paramyxovirus HN. Therefore, neuraminidase may have been introduced before the paramyxovirus-morbillivirus diversification. Thus, it is possible that the neuraminidase gene was introduced in influenza virus before the diversification of types A and B and the gene was introduced in *Paramyxoviridae*

before the diversification of respiroviruses, rubulaviruses, and morbilliviruses. Influenza virus N, paramyxovirus HN, and morbillivirus H have independently acquired a domain that elevated the neuraminidase head above the viral membrane. The very dissimilar stem regions of paramyxovirus HN compared with those of morbillivirus H suggest that the evolution of the stem occurred independently, after shared features like cystine bridges and the large β3L23 loop had evolved.

We discovered neuraminidase activity in RPV and PPRV. RPV has been suggested to be the archetype morbillivirus (46). This neuraminidase activity is independent of divalent cations, has a pH optimum typical for viral neuraminidases, is not blocked by the most common neuraminidase inhibitor (DANA), and is highly substrate specific. The high substrate specificity may be related to the inability to be inhibited by DANA. We detected the substrate only in crude mucins from bovine submaxillary glands. The exact type of sialic acid serving as the RPV H substrate remains to be elucidated. Except for a slight activity with PPRV, the other morbilliviruses did not show any neuraminidase activity with this substrate. Perhaps species-specific substrates exist for the other morbillivirus neuraminidases. Most differences in the morbillivirus active sites are found on the opposite face of the glycosidic bond where interactions occur with the sialic acid glycerol side chain in influenza virus neuraminidase. This suggests that the substrate for morbillivirus neuraminidases may be sialic acids with typical modifications at the 5 or 6 position.

Influenza virus neuraminidase, paramyxovirus hemagglutinin-neuraminidase, and morbillivirus hemagglutinin are named after their identified properties. However, because we identified neuraminidase activity in a morbillivirus and because hemagglutinin activity has been observed in several influenza virus neuraminidase proteins (18, 31), the different names for these topologically similar proteins are confusing. The general function for all these proteins may be similar and versatile: neuraminidase activity, carbohydrate binding and/or receptor binding, and in some cases binding to the neighboring fusion protein. The similarities in structure and function may generalize aspects of the infection mechanism. It is likely that microorganisms that infect the respiratory tract have evolved a way to migrate through the mucus layer. Binding of virus to the receptor is considered to be a multistep process (19). Multiple receptors could be coreceptors and act together, or the receptors may act sequentially. Virus binding might involve a rapid low-affinity interaction with an abundant receptor, such as terminal sialic acids on mucin polymers. A virus with a hemagglutinin and glycosidase activity, like the orthomyxoviruses and the *Paramyxoviridae*, could then roll over or swim through a mucus layer by continuously binding and cleaving sialic acid. After browsing the abundant low-affinity receptor environment, it might reach the cell surface and find the second, high-affinity receptor. Sialic acids ensure the viscoelastic properties of mucins. Therefore, mucus gels may be disintegrated, as was shown by the action of purified *Streptococcus pneumoniae* neuraminidase on mucins which resulted in a significant reduction in the native viscoelastic properties of the mucins (48). Perhaps microorganisms that have to cope with the mucus barrier evolved ways to overcome this barrier with glycosidic activity, esterase activity, or mucin-like regions (29). According to this hypothesis, it would be unusual if the morbilliviruses had no glycosidic activity. Like neuraminidase specificity in bacteria, the neuraminidase specificity may be related to the site of infection (10). The 3D models for *Paramyxoviridae* HN and H may guide functional studies. The discovered enzymatic activity of some morbillivirus H proteins provides new potential targets for therapeutic drugs.

ACKNOWLEDGMENTS

We thank Wouter Puijk and Frans Rijsewijk for helpful discussions.

REFERENCES

1. **Aymard-Henry, M., M. T. Coleman, E. R. Dowdle, W. G. Laver, G. C. Schild, and R. G. Webster.** 1973. Influenzavirus neuraminidase and neuraminidase-inhibition test procedures. Bull. W. H. O. **48:**199–202.
2. **Baty, D. U., and R. E. Randall.** 1993. Multiple amino acid substitutions in the HN protein of the paramyxovirus, SV 5, are selected for in monoclonal antibody resistant mutants. Arch. Virol. **131:**217–224.
3. **Bousse, T., T. Takimoto, W. L. Gorman, T. Takahashi, and A. Portner.** 1994. Regions on the hemagglutinin-neuraminidase proteins of human parainfluenza virus type-1 and Sendai virus important for membrane fission. Virology **204:**506–514.
4. **Burmeister, W. P., B. Henrissat, C. Bosso, S. Cusack, and R. W. H. Ruigrok.** 1993. Influenza B virus neuraminidase can synthesize its own inhibitor. Structure **1:**19–26.
5. **Cattaneo, R., and J. K. Rose.** 1993. Cell fusion by the envelope glycoproteins of persistent measles viruses which caused lethal human brain disease. J. Virol. **67:**1493–1502.
6. **Coelingh, K. J., C. C. Winter, B. R. Murphy, J. M. Rice, P. C. Kimball, R. A. Olmsted, and P. L. Collins.** 1986. Conserved epitopes on the hemagglutinin-neuraminidase proteins of human and bovine parainfluenza type 3 viruses: nucleotide sequence analysis of variants selected with monoclonal antibodies. J. Virol. **60:**90–96.
7. **Collins, P. L.** 1991. The molecular biology of human respiratory syncytial virus (RSV) of genus *Pneumovirus*, p. 103–162. *In* D. W. Kingsbury (ed.), The paramyxoviruses. Plenum Publishing Corp., New York, N.Y.
8. **Collins, P. L., and G. Mottet.** 1991. Homooligomerization of the hemagglutinin-neuraminidase glycoprotein of human parainfluenza virus type 3 occurs before the acquisition of correct intramolecular disulfide bonds and mature immunoreactivity. J. Virol. **65:**2362–2371.
9. **Colman, P. M., P. A. Hoyne, and M. C. Lawrence.** 1993. Sequence and structure alignment of paramyxovirus hemagglutinin-neuraminidase with influenza virus neuraminidase. J. Virol. **67:**2972–2980.
10. **Corfield, T.** 1992. Bacterial sialidases—roles in pathogenicity and nutrition. Glycobiology **2:**509–521. (Minireview.)
11. **Crennell, S., E. Garman, G. Laver, E. Vimr, and G. Taylor.** 1994. Crystal structure of Vibrio cholerae neuraminidase reveals dual lectin-like domains in addition to the catalytic domain. Structure **2:**535–544.
12. **Crennell, S. J., E. F. Garman, W. Greame Laver, E. R. Vimr, and G. L. Taylor.** 1993. Crystal structure of a bacterial sialidase (from Salmonella typhimurium LT2) shows the same fold as an influenza virus neuraminidase. Proc. Natl. Acad. Sci. USA **90:**9852–9856.
13. **Deng, R., Z. Wang, A. M. Mirza, and R. M. Iorio.** 1995. Localization of a domain on the paramyxovirus attachment protein required for the promotion of cellular fusion by its homologous fusion protein spike. Virology **209:**457–469.
14. **Devereux, J., P. Haeberli, and O. Smithies.** 1984. A comprehensive set of sequence analysis programs for the VAX. Nucleic Acids Res. **12:**387–395.
15. **Dorig, R. E., A. Marcil, A. Chopra, and C. D. Richardson.** 1993. The human CD46 molecule is a receptor for measles virus (Edmonston strain). Cell **75:**295–305.
16. **Enders, J. F., and T. C. Peebles.** 1954. Propagation in tissue cultures of cytopathogenic agents from patients with measles. Proc. Soc. Exp. Biol. Med. **86:**277–286.
17. **Feng, Y., C. C. Broder, P. E. Kennedy, and E. A. Berger.** 1996. HIV-1 entry cofactor: functional cDNA cloning of a seven-transmembrane, G protein-coupled receptor. Science **272:**872–877.
18. **Hausmann, J., E. Kretzschmar, W. Garten, and H. D. Klenk.** 1995. N1 neuraminidase of influenza virus A/FPV/Rostock/34 has haemadsorbing activity. J. Gen. Virol. **76:**1719–1728.
19. **Haywood, A. M.** 1994. Virus receptors: binding, adhesion strengthening, and changes in viral structure. J. Virol. **68:**1–5.
20. **Hu, A., H. Sheshberadaran, E. Norrby, and J. Kövamees.** 1993. Molecular characterization of epitopes on the measles virus hemagglutinin protein. Virology **192:**351–354.
21. **Hu, A., R. Cattaneo, S. Schwartz, and E. Norrby.** 1994. Role of N-linked oligosaccharide chains in the processing and antigenicity of measles virus hemagglutinin protein. J. Gen. Virol. **75:**1043–1052.
22. **Hu, X., R. Ray, and R. W. Compans.** 1992. Functional interactions between the fusion protein and hemagglutinin-neuraminidase of human parainfluenza viruses. J. Virol. **66:**1528–1534.
23. **Hummel, K. B., and W. J. Bellini.** 1995. Localization of monoclonal antibody epitopes and functional domains in the hemagglutinin protein of measles virus. J. Virol. **69:**1913–1916.
24. **Iorio, R. M., R. L. Glickman, A. M. Riel, J. P. Sheenan, and M. A. Bratt.** 1989. Identification of amino acid residues important to the neuraminidase activity of the glycoprotein of the Newcastle disease virus. Virology **173:**196–204.
25. **Iorio, R. M., R. J. Syddall, J. P. Sheehan, M. A. Bratt, R. L. Glickman, and**

A. M. Riel. 1991. Neutralization map of the hemagglutinin-neuraminidase glycoprotein of Newcastle disease virus: domains recognized by monoclonal antibodies that prevent receptor recognition. J. Virol. **65:**4999–5006.
26. **Jorgensen, E. D., P. L. Collins, and P. T. Lomedico.** 1987. Cloning and nucleotide sequence of Newcastle disease virus hemagglutinin-neuraminidase mRNA: identification of a putative sialic acid binding site. Virology **156:**12–24.
27. **Kingsbury, D. W., M. A. Bratt, P. W. Choppin, R. P. Hanson, Y. Hosaka, V. ter Meulen, E. Norrby, W. Plowright, R. Rott, and W. H. Wunner.** 1978. Paramyxoviridae. Intervirology **10:**137–152.
28. **Lamb, R. A.** 1993. Paramyxovirus fusion: a hypothesis for changes. Virology **197:**1–11.
29. **Langedijk, J. P. M., W. M. M. Schaaper, R. H. Meloen, and J. T. van Oirschot.** 1996. Proposed three-dimensional model for attachment protein G of respiratory syncytial virus. J. Gen. Virol. **77:**1249–1257.
30. **Lapthorn, A. J., R. W. Janes, N. W. Isaacs, and B. A. Wallace.** 1995. Cystine nooses and protein specificity. Nature Struct. Biol. **2:**266–268.
31. **Laver, W. G., P. M. Colman, R. G. Webster, V. S. Hinshaw, and G. M. Air.** 1984. Influenza virus neuraminidase with hemagglutinin activity. Virology **137:**314–323.
32. **Lecouturier, V., J. Fayolle, M. Caballero, J. Carabana, M. L. Celma, R. Fernandez-Munoz, T. F. Wild, and R. Buckland.** 1996. Identification of two amino acids in the hemagglutinin glycoprotein of measles virus (MV) that govern hemadsorption, HeLa cell fusion, and CD46 downregulation: phenotypic markers that differentiate vaccine and wild-type MV strains. J. Virol. **70:**4200–4204.
33. **Liebert, U. G., S. G. Flanagan, S. Löffler, K. Baczko, V. ter Meulen, and B. K. Rima.** 1994. Antigenic determinants of measles virus hemagglutinin associated with neurovirulence. J. Virol. **68:**1486–1493.
34. **Mackay, H. J., A. J. Cross, and A. T. Hagler.** 1989. The role of energy minimization in simulation strategies of biomolecular systems, p. 340. *In* G. D. Fasman (ed.), Prediction of protein structure and the principle of protein conformation. Plenum Press, New York, N.Y.
35. **Mäkelä, M. J., G. A. Lund, and A. A. Salmi.** 1989. Antigenicity of the measles virus haemagglutinin studied by using synthetic peptides. J. Gen. Virol. **70:**603–614.
36. **Mäkelä, M. J., A. A. Salmi, E. Norrby, and T. F. Wild.** 1989. Monoclonal antibodies against measles virus haemagglutinin react with synthetic peptides. Scand. J. Immunol. **30:**225–231.
37. **Malvoisin, E., and T. F. Wild.** 1993. Measles virus glycoproteins: studies on the structure and interaction of the hemagglutinin and fusion proteins. J. Gen. Virol. **74:**2365–2372.
38. **McGinnes, L. W., and T. G. Morrison.** 1994. Modulation of the activities of HN protein of Newcastle disease virus by nonconserved cysteine residues. Virus Res. **34:**305–316.
39. **McGinnes, L. W., and T. G. Morrison.** 1994. Conformationally sensitive antigenic determinants on the HN glycoprotein of Newcastle disease virus form with different kinetics. Virology **199:**255–264.
40. **McGinnes, L. W., and T. G. Morrison.** 1994. The role of the individual cysteine residues in the formation of the mature, antigenic HN protein of Newcastle disease virus. Virology **200:**470–483.
41. **Mirza, A. M., J. P. Sheenan, L. W. Hardy, R. L. Glickman, and R. M. Iorio.** 1993. Structure and function of a membrane anchor-less form of the hemagglutinin-neuraminidase glycoprotein of Newcastle disease virus. J. Biol. Chem. **268:**21425–21431.
42. **Miyagi, T., K. Konno, Y. Emor, H. Kawasaki, K. Suzuki, A. Yasui, and S. Tsuiki.** 1993. Molecular cloning and expression of a cDNA encoding rat skeletal muscle cytosolic sialidase. J. Biol. Chem. **268:**26435–26440.
43. **Naniche, D., G. Varior-Krishnan, F. Cervoni, T. F. Wild, B. Rossi, C. Rabourdin-Combe, and D. Gerlier.** 1993. Human membrane cofactor protein (CD46) acts as a cellular receptor for measles virus. J. Virol. **67:**6025–6032.
44. **Ng, D. T. W., R. E. Randall, and R. A. Lamb.** 1989. Intracellular maturation and transport of the SV5 type II glycoprotein hemagglutinin-neuraminidase: specific and transient association with GRP78-BiP in the endoplasmic reticulum and extensive internalization from the cell surface. J. Cell Biol. **109:**3273–3289.
45. **Niefind, K., and D. Schomburg.** 1991. Amino acid similarity coefficients for protein modeling and sequence alignment derived from main-chain folding angles. J. Mol. Biol. **219:**481–497.
46. **Norrby, E., H. Sheshberadaran, K. C. McCullough, W. C. Carpenter, and C. Orvell.** 1985. Is rinderpest virus the archevirus of the morbillivirus genus? Intervirology **23:**228–232.
47. **Palese, P., K. Tobita, M. Ueda, and R. W. Compans.** 1974. Characterization of temperature-sensitive influenza virus mutants defective in neuraminidase. Virology **61:**397–410.
48. **Puchelle, E., F. Girard, N. Houdret, and V. Bailleul.** 1975. Action des neuraminidases de Diplococcus pneumonaie et de Clostridum perfringens sur les propriétés visco-élastiques des sécrétions bronchiques. Biorheology **12:**219–224.
49. **Richman, A. V., F. A. Pedeira, and N. M. Tauraso.** 1971. Attempts to demonstrate hemagglutination and hemadsorption by respiratory syncytial virus. Appl. Microbiol. **21:**1099–1100.
50. **Roggentin, P., R. Schauer, L. L. Hoyer, and E. R. Vimr.** 1993. The sialidase superfamily and its spread by horizontal gene transfer. Mol. Microbiol. **9:**915–921.
51. **Rost, B., and C. Sander.** 1992. Jury returns on structure prediction. Nature **360:**540.
52. **Sergel, T., L. W. McGinnes, M. E. Peeples, and T. G. Morrison.** 1993. The attachment function of the Newcastle disease virus hemagglutinin-neuraminidase protein can be separated from fission promotion by mutation. Virology **193:**717–726.
53. **Sheshberadaran, H., and E. Norrby.** 1986. Characterization of epitopes on the measles virus hemagglutinin protein. Virology **152:**58–65.
54. **Shibahara, K., H. Hotta, Y. Katayama, and M. Homma.** 1994. Increased binding activity of measles virus to monkey red blood cells after longterm passage in Vero cell cultures. J. Gen. Virol. **75:**3511–3516.
55. **Thompson, S. D., W. G. Laver, K. G. Murti, and A. Portner.** 1988. Isolation of a biologically active soluble form of from the hemagglutinin-neuraminidase protein of Sendai virus. J. Virol. **62:**4653–4660.
56. **Varghese, J. N., W. G. Laver, and P. M. Colman.** 1983. Structure of the influenza virus glycoprotein antigen neuraminidase at 2.9 Å resolution. Nature **303:**35–40.
57. **Von A. Mayr, P. A. Bachmann, B. Bibrack, and G. Wittmann.** 1974. Virologische Arbeitsmethoden, p. 254. VEB Gustav Fischer Verlag, Jena, Germany.
58. **Ward, C. W., T. C. Elleman, and A. A. Azad.** 1982. Amino acid sequence of the pronase-released heads of neuraminidase subtype N2 from Asian strain A/Tokyo/3/67 of influenza virus. Biochem. J. **207:**91–95.
59. **Ziegler, D., P. Fournier, G. A. H. Berbers, H. Steuer, K. H. Wiesmüller, B. Fleckenstein, F. Schneider, G. Jung, C. C. King, and C. P. Muller.** 1996. Protection against measles virus encephalitis by monoclonal antibodies binding to a cystine loop domain of the H protein mimicked by peptides which are not recognized by maternal antibodies. J. Gen. Virol. **77:**2479–2489.